

Exoplanetary Transit Constraints Based upon Secondary Eclipse Observations

STEPHEN R. KANE AND KASPAR VON BRAUN

NASA Exoplanet Science Institute, California Institute of Technology, Pasadena, CA 91125; skane@ipac.caltech.edu

Received 2009 July 15; accepted 2009 August 4; published 2009 September 9

ABSTRACT. Transiting extrasolar planets provide an opportunity to study the mass-radius relation of planets as well as their internal structure. The existence of a secondary eclipse enables further study of the thermal properties of the planet by observing at infrared wavelengths. The probability of an observable secondary eclipse depends upon the orbital parameters of the planet, particularly eccentricity and argument of periastron. Here we provide analytical expressions for these probabilities, investigate their properties, and calculate their values for the known extrasolar planets. We furthermore quantitatively discuss constraints on existence and observability of primary transits if a secondary eclipse is observed. Finally, we calculate the a posteriori transit probabilities of the known extrasolar planets, and we present several case studies in which orbital constraints resulting from the presence of a secondary eclipse may be applied in observing campaigns.

1. INTRODUCTION

Transiting planet discoveries have become an integral component of the extrasolar planets field, with discoveries taking place at an ever-increasing rate. The additional information provided by the detection of a transit to the overall understanding of both the orbital elements and the planetary properties is invaluable. In particular, data acquired through the observations of secondary eclipses has allowed an unprecedented insight into the analysis of planetary atmospheres (Burrows et al. 2005, 2006; Grillmair et al. 2008; Knutson et al. 2007; Williams et al. 2006). These secondary eclipses have been observed most notably from space (Deming et al. 2006, 2007a, 2007b) but have also been detected from the ground (de Mooij & Snellen 2009; Gillon et al. 2009; Sing & López-Morales 2009).

The effect of orbital parameters upon the probability of an observable primary transit has been discussed in detail by such papers as Barnes (2007) and Burke (2008). The effects of the eccentricity and argument of periastron have a considerable effect on this probability for many of the known planets discovered through the radial velocity method (Kane & von Braun 2008). An example of this is the planet orbiting HD 17156 whose relatively large eccentricity results in a high primary transit probability. Subsequent observing campaigns confirmed that this planet does indeed transit its parent star (Barbieri et al. 2007; Winn et al. 2009).

For a given eccentricity, the inverse case of a high primary transit probability is that of a high secondary eclipse probability. The case of HD 80606b (Naef et al. 2001) is a spectacular example with an orbital eccentricity of ~ 0.93 and argument of periastron of $\sim 300^\circ$, resulting in an especially high secondary eclipse probability, despite an orbital period of more than

111 days. The secondary eclipse was successfully detected by Laughlin et al. 2009 using the *Spitzer Space Telescope's* Infrared Array Camera. With the observation of a secondary eclipse, efforts were undertaken to determine if the planet also produces an observable primary transit. These efforts were eventually fruitful with the confirmation of a primary transit (Fossey et al. 2009; Garcia-Melendo & McCullough 2009; Moutou et al. 2009).

Despite a favorable orbital inclination, merely the presence of either a secondary eclipse or a primary transit does not necessarily imply that its counterpart will be detectable. If a secondary eclipse is observed for a known radial velocity planet (as was the case for HD 80606b) then the likelihood of a primary transit is increased. However, exactly how likely this primary transit is will inform the justification for mounting an exhaustive follow-up campaign. Here we calculate secondary eclipse probabilities for known radial velocity planets, and show how improved estimates on primary transit probabilities can be made and predicted transit midpoints can be placed if a secondary eclipse is observed. We further demonstrate this with several case studies which apply these constraints to some of the known radial velocity planets.

2. SECONDARY ECLIPSES

In this section we calculate secondary eclipse probabilities and apply it to the known radial velocity planets. We also discuss the limitations of impact parameter measurements and subsequent uncertainties in the estimation of the orbital inclination from secondary eclipse observations. In this and all subsequent sections, we use t and e as subscripts for (primary) transit and (secondary) eclipse, respectively.

2.1. Geometric Eclipse Probability

The geometric transit probability, P_t , is often approximated as the ratio of the radius of the parent star, R_* , to the semimajor axis of the planetary orbit, a . A more thorough consideration of the orbital parameters shows that the probability of a primary transit can be more accurately described by

$$P_t = \frac{(R_p + R_*)[1 + e \cos(\pi/2 - \omega)]}{a(1 - e^2)}, \quad (1)$$

where R_p is the radius of the planet, e is the eccentricity, and ω is the argument of periastron. The effects of e and ω upon the transit probability can be considerable, as shown by Kane & von Braun (2008). This probability peaks where $\omega = \pi/2$.

The true anomaly, f , is defined as the angle between the current position of the planet in its orbit and the direction of periapsis. The location in the orbit at which the planet crosses a plane between the host star and the observer that is perpendicular to the orbit is where a primary transit can occur, and is where $\omega + f = \pi/2$ (Kane 2007). If we extend the star-observer plane beyond the host star, the location where the planet crosses the plane on the far side of the star is where $\omega + f = 3\pi/2$ and is the location where it is possible for for a secondary eclipse to occur. Hence the geometric eclipse probability, P_e , is given by

$$P_e = \frac{(R_p + R_*)[1 + e \cos(3\pi/2 - \omega)]}{a(1 - e^2)}. \quad (2)$$

This probability peaks where $\omega = 3\pi/2$.

Depending upon the orientation of an eccentric orbit, it is possible for planets to have both a higher transit and eclipse probability than that produced by a circular orbit with the same period. In other words, there is a range of periastron arguments for which the projected star-planet separation

$$r = \frac{a(1 - e^2)}{1 + e \cos f} \quad (3)$$

is smaller than that for a circular orbit with the same period both in front of and behind the star along the line of sight. This is demonstrated in Figure 1, which shows three different orbital orientations relative to the line of sight of an observer (indicated by the arrow). The periastron arguments of orbits a, b, and c are π , $\pi/2$, and $\pi/4$, respectively. This visualization of the various configurations clearly shows how the star-planet separation along the line of sight is dependent on the argument of periastron and subsequently affects both the transit and eclipse probabilities.

Figure 2 shows the dependence of transit and eclipse probability upon periastron argument for an eccentricity of 0.6, along with those regions for which both probabilities exceed that of a corresponding circular orbit (shaded regions). The stellar mass and radius are assumed to be solar mass and

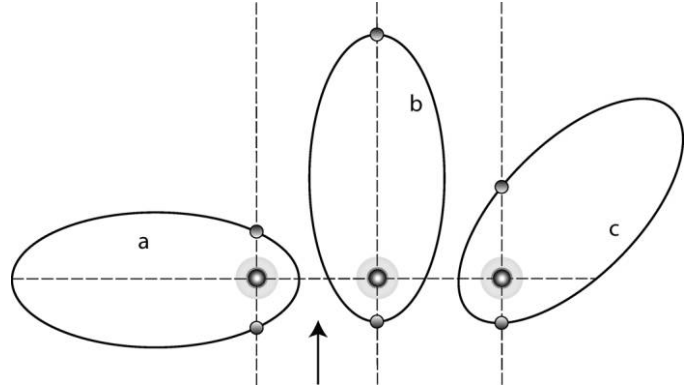


FIG. 1.—Top-down view of three different orbital configurations of an eccentric orbit, with the arrow indicating the line of sight of an observer. The periastron arguments of orbits a, b, and c are π , $\pi/2$, and $\pi/4$ respectively. The star-planet distance both in front of and behind the star is highly dependent upon this periastron argument.

radius, respectively, while the planet is assumed to have a Jupiter radius. For this particular eccentricity, the shaded regions account for 40% of the possible periastron arguments. It is often nonintuitive that there exist orbital configurations where both probabilities are enhanced, since they are often assumed to have inverse relation to each other.

The total size of the shaded regions depends upon the eccentricity of the orbit and can be calculated analytically by considering those values of ω for which the transit probability of a circular orbit equals that of an eccentric orbit for the same period. Using equation (3), this is where

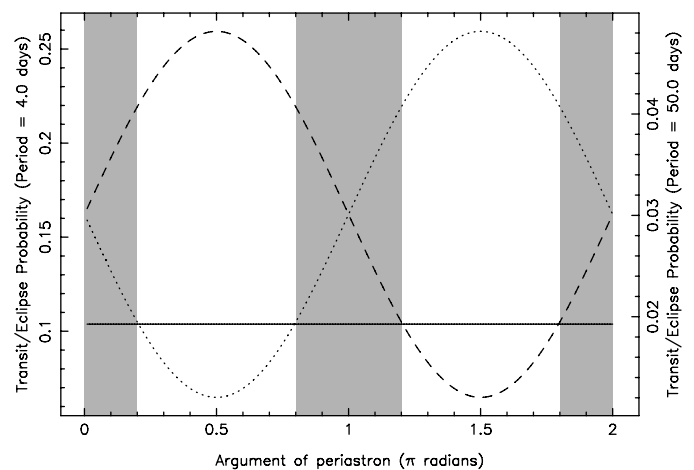


FIG. 2.—Dependence of geometric transit (*dashed line*) and eclipse (*dotted line*) probability on the argument of periastron for an eccentricity of 0.6 (see eqs. [1] and [2]). The *solid line* indicates the probabilities for a circular orbit with the same orbital period. These are plotted for periods of 4.0 days (left ordinate) and 50.0 days (right ordinate). Stellar and planetary radii are assumed to be a Jupiter and solar radius, respectively. The *shaded regions* represent those ranges of periastron arguments for which both the transit and eclipse probabilities exceed that of a circular orbit.

$$\frac{a(1 - e_0^2)}{1 + e_0 \cos f} = \frac{a(1 - e^2)}{1 + e \cos f} \quad (4)$$

which yields

$$f = \pm \cos^{-1}(-e) \quad (5)$$

when $e_0 = 0$ (circular orbit). The values of ω which define the boundaries of the shaded regions in Figure 2 are then given by $\omega + f = \pi/2$ and $\omega + f = 3\pi/2$ for primary transits and secondary eclipses, respectively. The total size of the shaded regions $\Delta\omega$ can then be expressed as

$$\Delta\omega = 4 \cos^{-1}(-e) - 2\pi. \quad (6)$$

Figure 3 shows the dependence of the value of $\Delta\omega$ on the eccentricity of the orbit. According to Burke (2008), the mean eccentricity of the known extrasolar planets is ~ 0.3 for orbital periods greater than 10 days. This is indicated on Figure 3 as a dashed line which shows that almost 20% of the ω values for this eccentricity will have higher transit/eclipse probabilities than for a circular orbit with the same period. The eccentricity for which half of the ω values fall into this category is also shown as a dotted line. This occurs when the magnitude of the eccentricity exceeds ~ 0.71 . This can be used to identify planets for which observations at both predicted transit and eclipse times would be beneficial to make efficient use of observing time. In general, if the value of e has been measured, then the value of ω will also have an associated estimate which will define exactly where on Figures 2 and 3 the planet lies. It should also be noted that a high probability of both transit and eclipse provides access to greater

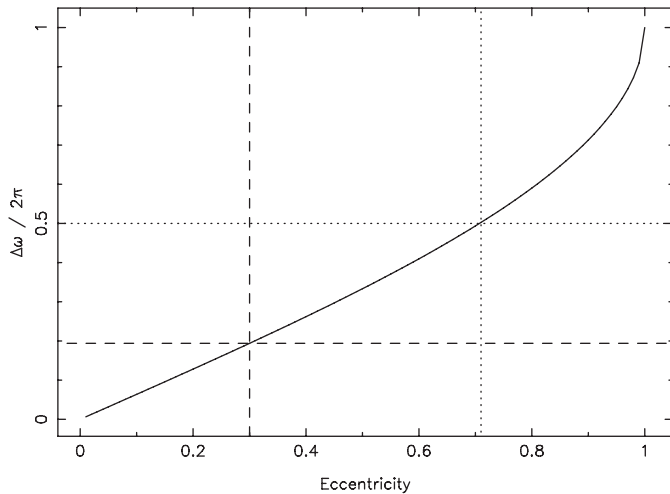


FIG. 3.—Dependence of the fractional range of periastron arguments for which both the transit and eclipse probabilities exceed that of a circular orbit with the same period (shaded regions in Fig. 2) on the orbital eccentricity. The *dashed lines* correspond to $e = 0.3$ and the *dotted lines* correspond to $\Delta\omega/2\pi = 0.5$.

science opportunities. A transit passage primarily enables measurement of the planetary radius, whereas an eclipse passage primarily enables measurement of the planetary flux which, when combined with planetary atmosphere models, can lead to an estimate of the planetary temperature.

Kane & von Braun (2008) used the orbital parameters provided by Butler et al. (2006) to calculate the primary transit probabilities for 203 planets. These calculations took into account the eccentricity and argument of periastron to demonstrate the inflated probabilities that can occur as a result. In Figure 4 we show the results of performing a similar calculation using the same data to estimate secondary eclipse probabilities. We assume a Jupiter and Solar radius for the values of R_p and R_* respectively to provide ease of comparison with the eclipse probability of a circular orbit with the same period, shown as a solid curve. Note that there are a handful of M dwarfs in the sample whose eclipse probabilities will be a factor of 2 lower than those shown in the figure due to the assumption regarding stellar radius.

The secondary eclipse probability of HD 80606b is labeled in Figure 4. Since HD 80606 is of solar-type (G5V) and the planet is approximately the same size as Jupiter, the indicated probability is close to the true probability for this planet. The residuals show that the increase in eclipse probability for this planet compared to a circular orbit with the same period is $>15\%$. Apart from HD 80606b and a few outliers at periods <100 days, another example of an unexpectedly high P_t in this plot is the long-period planet HD 4113b (Tamuz et al. 2008). This planet has a period of 526.62 days and an eccentricity of 0.903. Such a high eccentricity means that, according to

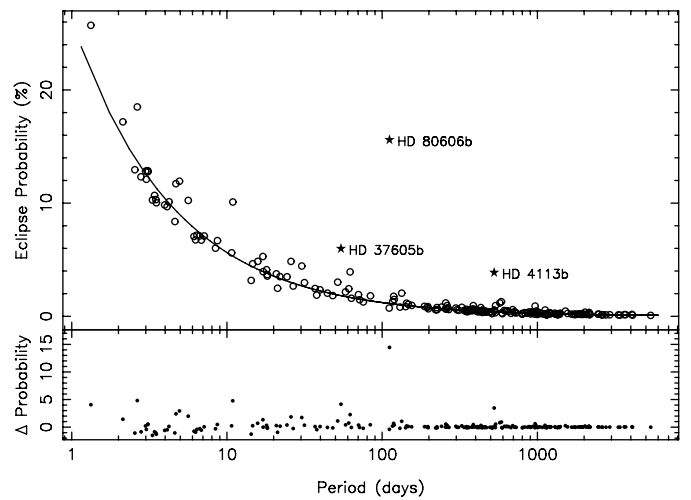


FIG. 4.—The geometric eclipse probability for a circular orbit with the published period (solid curve) along with the eclipse probability for 203 RV planets from Butler et al. (2006) calculated from their orbital parameters (*open circles*). HD 80606b, HD 4113b, and HD 37605b (*stars*) are examples of particularly high eclipse probabilities. The lower panel plots the difference in P_t between the actual orbit and a hypothetical circular orbit with the same period for each of the planets.

Figure 3, $\sim 70\%$ of the possible values of ω will result in both a higher transit and a higher eclipse probability than if the eccentricity were zero. Thus, even though the periastron argument is $\omega = 317.7^\circ$, the secondary eclipse probability is still raised by 3.5% compared to the corresponding circular orbit.

2.2. Impact Parameter and Inclination

Here we show how the existence of a secondary eclipse can constrain values of the impact parameter and orbital inclination angle. The dimensionless impact parameter, b , of an exoplanetary transit is defined as the projected separation of the planet and star centers at the point of midtransit. Thus b is related to the inclination, i , by

$$b \equiv \frac{r}{R_\star} \cos i \quad (7)$$

such that $0 \leq b \leq 1$. In equation (7), we have generalized from a circular to an eccentric orbit by replacing a with r . As discussed in detail by Seager & Mallén-Ornelas (2003), the measured impact parameter is highly dependent upon the shape of the light curve, in particular the duration of ingress and egress. Seager & Mallén-Ornelas (2003) also point out that b will typically be underestimated when there is relatively low signal-to-noise in the transit data. This will be true for almost all ground-based observations of secondary eclipses, and is even sometimes true for Spitzer secondary eclipse observations.

If we assume that the maximum secondary eclipse depth is achieved (the full disk of the planet passes behind the star), then b can be as high as $(R_\star - R_p)/R_\star$. The orbital inclination will then be as low as

$$i = \cos^{-1} \left(\frac{R_\star - R_p}{r_e} \right) \quad (8)$$

where r_e is the star-planet separation at eclipse (see eq. [3]). For a Jupiter-type planet orbiting a solar-type star with a period of 4 days, this results in a maximum impact parameter of $b \sim 0.9$ and hence a minimum orbital inclination of $i \sim 85^\circ$. For HD 80606b, the orbital parameters of $e = 0.9336$ and $\omega = 300.4977^\circ$ (Fossey et al. 2009), lead to a star-planet separation of $r_e = 0.032$ AU mid-eclipse and $r_t = 0.297$ AU at midtransit. Adopting the stellar and planetary radii used by Fossey et al. (2009), the minimum inclination for this planet is $i = 82.5^\circ$.

3. PRIMARY TRANSIT CONSTRAINTS

In this section we show the impact the detection of a secondary eclipse has on the predictions regarding an observable primary transit of the planet.

3.1. Geometric Transit Probability

In most cases, an estimate of a planet's primary transit probability is made with no knowledge of the planet's orbital inclination. However, the constraints on the inclination discussed in the previous section allow for an improved estimate of the primary transit probability. Since the minimum inclination can be calculated from the presence of a secondary eclipse, the probability of a primary transit is given by

$$P_t \geq \frac{R_p + R_\star}{r_t \cos i}. \quad (9)$$

Note the inequality used in this equation to make it clear that this represents a lower limit on the true transit probability. Using equation (8), this probability may be re-expressed as

$$P_t \geq \frac{(R_\star + R_p) r_e}{(R_\star - R_p) r_t}, \quad (10)$$

thus removing the inclination dependence. Generally speaking, if $r_e > r_t$ then a secondary eclipse detection almost guarantees that a primary transit will also be observable. By substituting Equation 3 and using trigonometric identities, the probability may be re-expressed once again as

$$P_t \geq \frac{(R_\star + R_p)(1 + e \sin \omega)}{(R_\star - R_p)(1 - e \sin \omega)}, \quad (11)$$

which removes dependence upon semimajor axis or period, and replaces these with the dependence upon eccentricity and periastron argument.

Figure 5 demonstrates the improvement one gains in the primary transit probability if a secondary eclipse is detected as a function of both eccentricity and periastron argument. This demonstration uses the same orbital parameters for the 203 planets shown in Figure 4 as provided by Butler et al. (2006). As for Figure 4, Jupiter and solar radii are assumed for the planetary and host star radii respectively. The open circles are the transit probabilities calculated using equation (1), which assumes no prior knowledge regarding the inclination of the planetary orbit. The crosses are the revised transit probabilities calculated from equation (11), which assumes that a secondary eclipse has been observed. The 50 planets with highest probability of eclipse in this sample are tabulated in Table 1 along with basic orbital parameters and their original and revised transit probabilities.

Figure 5 and Table 1 show that for many cases, the transit probability is elevated to 100% when a secondary eclipse is observed; indeed this is true for almost 75% of the planets included in this sample. Figure 5, left panel, indicates that the transit probability for the stars with a postulated observation of secondary eclipse (crosses) fans out for $e > 0.1$ with an envelope whose lower edge appears linear with a negative slope. The

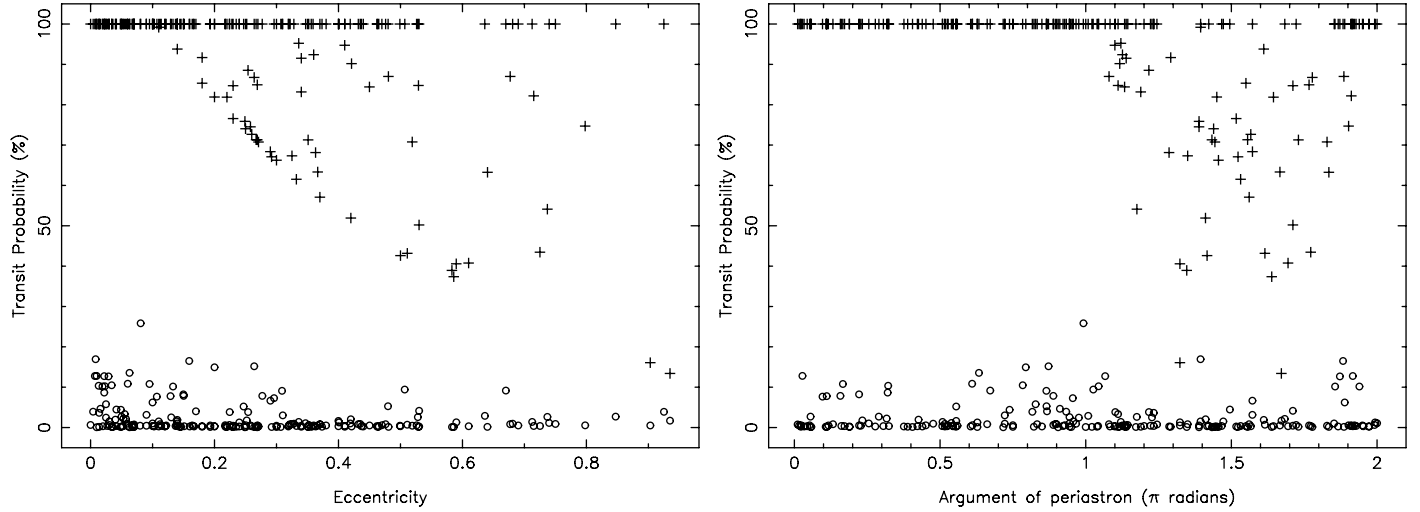


Fig. 5.—The original (eq. [11]) and revised (eq. [11]) primary transit probabilities for 203 planets from the Butler et al. (2006) catalog, plotted as a function of eccentricity and argument of periastron. The original probabilities are shown as *open circles* and the revised (when a secondary eclipse is detected) probabilities are shown as *crosses*.

right panel demonstrates that if the argument of periastron is close to $\pi/2$, then one can be assured of an observable primary transit based upon a secondary eclipse. However, if the argument of periastron is close to $3\pi/2$, then a noncircular orbit will correspondingly reduce this improvement to the transit probability. This region corresponds to the region of high secondary eclipse probability shown in Figure 2.

3.2. Expected Primary Transit Time

If a secondary eclipse is observed, then how long will it be before the expected time of primary transit occurs? Can the necessary observing resources be acquired or alerted in time to perform the observations? What will be the size of the transit window and can the observations be justified with regard to the uncertainty in the transit midpoint, the predicted transit duration, and the transit probability? These are all fair questions to ask when planning a follow-up campaign in the wake of a secondary eclipse detection, especially in light of the deteriorating precision of the transit ephemerides with time.

The predicted time of midtransit can be calculated by utilizing Kepler's equations. Firstly, the eccentric anomaly is calculated from the following relation to the true anomaly

$$E = 2 \tan^{-1} \left(\sqrt{\frac{1-e}{1+e}} \tan \frac{f}{2} \right). \quad (12)$$

The mean anomaly, M , which defines the time since last periastris in units of radians, is then computed by

$$M = E - e \sin E \quad (13)$$

which can be converted to regular time units using

$$t_M = \frac{PM}{2\pi}. \quad (14)$$

By substituting $\omega + f = \pi/2$ and $\omega + f = 3\pi/2$ into equation (12), we can calculate the predicted times of primary transit, t_t , and secondary eclipse, t_e , respectively

$$t_t = t_{\text{peri}} + t_M|_{(\omega+f=\pi/2)} \quad (15)$$

$$t_e = t_{\text{peri}} + t_M|_{(\omega+f=3\pi/2)} \quad (16)$$

where t_{peri} is the time of periastron passage. These times can then be combined to yield the predicted time of primary transit as a function of secondary eclipse

$$t_t = t_e + \frac{P}{2\pi} (M_t - M_e) + nP \quad (17)$$

where M_t and M_e are the mean anomalies for primary transit and secondary eclipse respectively. This equation is true for $-\pi/2 \leq \omega \leq \pi/2$, with an additional period needing to be added for $\pi/2 \leq \omega \leq 3\pi/2$. The term of $n \times P$ can be used to calculate an ephemeris where n is the number of complete orbits one would like to consider. As expected, equation (17) reduces to $t_t = t_e + P/2$ when $e = 0$.

The uncertainties in the orbital parameters can be propagated through these equations to determine the size of the transit window. Under normal circumstances, the size of a transit window is most dependent upon the uncertainty in the period and the time elapsed since last observations were acquired. However, if a secondary eclipse has been observed then the constraints on the window tighten and become dominated by the eccentricity.

TABLE 1
THE 50 HIGHEST ECLIPSE PROBABILITY PLANETS
FROM THE BUTLER ET AL. (2006) SAMPLE

| Planet | P (days) | e | ω ($^{\circ}$) | P_t (%) | P_e (%) | P'_t (%) |
|---------------|---------------|------|----------------------------|--------------|--------------|---------------|
| HD 41004 B b | 1.33 | 0.08 | 178.50 | 25.81 | 25.70 | 100.00 |
| GJ 436 b | 2.64 | 0.16 | 339.00 | 16.50 | 18.50 | 100.00 |
| HD 86081 b | 2.14 | 0.01 | 251.00 | 16.93 | 17.19 | 100.00 |
| HD 80606 b | 111.45 | 0.93 | 300.89 | 1.71 | 15.58 | 13.41 |
| HD 73256 b | 2.55 | 0.03 | 337.00 | 12.66 | 12.95 | 100.00 |
| HD 179949 b | 3.09 | 0.02 | 192.00 | 12.74 | 12.86 | 100.00 |
| HD 83443 b | 2.99 | 0.01 | 345.00 | 12.77 | 12.82 | 100.00 |
| HD 187123 b | 3.10 | 0.01 | 5.03 | 12.81 | 12.78 | 100.00 |
| 55 Cnc e | 2.80 | 0.26 | 157.00 | 15.17 | 12.33 | 100.00 |
| HD 46375 b | 3.02 | 0.06 | 114.00 | 13.58 | 12.11 | 100.00 |
| HD 49674 b | 4.94 | 0.29 | 283.00 | 6.68 | 11.94 | 68.37 |
| GJ 674 b | 4.69 | 0.20 | 143.00 | 14.93 | 11.72 | 100.00 |
| HD 88133 b | 3.42 | 0.13 | 349.00 | 10.16 | 10.68 | 100.00 |
| BD-10 3166 b | 3.49 | 0.02 | 334.00 | 10.15 | 10.32 | 100.00 |
| tau Boo b | 3.31 | 0.02 | 188.00 | 10.21 | 10.27 | 100.00 |
| HAT-P-2 b | 5.63 | 0.51 | 184.60 | 9.44 | 10.24 | 100.00 |
| 51 Peg b | 4.23 | 0.01 | 58.00 | 10.35 | 10.12 | 100.00 |
| HD 108147 b | 10.90 | 0.53 | 308.00 | 4.14 | 10.09 | 50.21 |
| HD 75289 b | 3.51 | 0.03 | 141.00 | 10.47 | 10.03 | 100.00 |
| HD 76700 b | 3.97 | 0.09 | 29.90 | 10.82 | 9.84 | 100.00 |
| HD 102195 b | 4.12 | 0.06 | 109.90 | 10.85 | 9.69 | 100.00 |
| upsilon And d | 4.62 | 0.02 | 57.60 | 8.69 | 8.38 | 100.00 |
| HD 168746 b | 6.40 | 0.11 | 17.40 | 7.63 | 7.16 | 100.00 |
| HD 217107 b | 7.13 | 0.13 | 20.00 | 7.76 | 7.11 | 100.00 |
| HIP 14810 b | 6.67 | 0.15 | 160.00 | 7.86 | 7.10 | 100.00 |
| HD 118203 b | 6.13 | 0.31 | 155.70 | 9.11 | 7.05 | 100.00 |
| HD 68988 b | 6.28 | 0.15 | 40.00 | 8.20 | 6.76 | 100.00 |
| HD 185269 b | 6.84 | 0.30 | 172.00 | 7.30 | 6.72 | 100.00 |
| HD 69830 b | 8.67 | 0.10 | 340.00 | 6.24 | 6.68 | 100.00 |
| HD 162020 b | 8.43 | 0.28 | 28.40 | 7.84 | 6.02 | 100.00 |
| HD 37605 b | 54.23 | 0.74 | 211.60 | 2.64 | 5.97 | 54.12 |
| HD 130322 b | 10.71 | 0.03 | 149.00 | 5.76 | 5.62 | 100.00 |
| HD 99492 b | 17.04 | 0.25 | 219.00 | 3.83 | 5.29 | 88.53 |
| HD 13445 b | 15.76 | 0.04 | 269.00 | 4.47 | 4.85 | 100.00 |
| HD 117618 b | 25.83 | 0.42 | 254.00 | 2.06 | 4.85 | 51.92 |
| 55 Cnc b | 14.65 | 0.02 | 164.00 | 4.67 | 4.63 | 100.00 |
| GJ 876 c | 30.34 | 0.22 | 198.30 | 3.85 | 4.44 | 100.00 |
| HD 27894 b | 17.99 | 0.05 | 132.90 | 4.43 | 4.12 | 100.00 |
| HD 3651 b | 62.24 | 0.59 | 238.20 | 1.30 | 3.93 | 40.58 |
| HD 190360 c | 17.11 | 0.00 | 168.00 | 3.94 | 3.93 | 100.00 |
| HD 4113 b | 526.62 | 0.90 | 238.20 | 0.51 | 3.86 | 16.08 |
| HD 102117 b | 20.81 | 0.09 | 283.00 | 3.14 | 3.74 | 100.00 |
| HD 195019 b | 18.20 | 0.01 | 222.00 | 3.62 | 3.69 | 100.00 |
| HD 33283 b | 18.18 | 0.48 | 155.80 | 5.31 | 3.56 | 100.00 |
| HD 6434 b | 22.00 | 0.17 | 156.00 | 4.02 | 3.50 | 100.00 |
| HD 192263 b | 24.36 | 0.05 | 200.00 | 3.36 | 3.49 | 100.00 |
| HD 38529 b | 14.31 | 0.25 | 100.00 | 5.21 | 3.17 | 100.00 |
| HD 74156 b | 51.64 | 0.64 | 181.50 | 2.91 | 3.01 | 100.00 |
| HD 69830 c | 31.56 | 0.13 | 221.00 | 2.51 | 2.97 | 100.00 |
| HD 224693 b | 26.73 | 0.05 | 10.00 | 2.72 | 2.68 | 100.00 |

NOTE.—Period, P ; eccentricity, e ; periastron argument, ω ; transit probability, P_t ; eclipse probability, P_e ; and the revised transit probabilities, P'_t , calculated from equation (11).

4. CASE STUDIES

There are several specific cases of known exoplanets for which it is useful to apply the principles described in § 3. We consider some of these cases here.

4.1. HD 80606b

HD 80606b (Naef et al. 2001) is the first planet whose secondary eclipse was discovered before its primary transit. As described in § 2.2, if we used the revised orbital parameters by Fossey et al. (2009), then the observation of a secondary eclipse places a constraint of $i = 82.5^{\circ}$ on the inclination of the orbit. The equations in § 5 yield an a posteriori primary transit probability of 13.4%. For comparison, the probability of a primary transit without any knowledge of the orbital inclination is 1.7%.

Using the equations in § 3.2, one can calculate the time between secondary eclipse and primary transit to be only 5.86 days; small compared to the 111.43 day period. Additionally, the time difference between secondary eclipse midpoint and periastron is 0.12 days (~ 3 hr), emphasizing the suitability of this system for secondary eclipse detection. This time difference yields a predicted transit midpoint of HJD 2454876.32 for the fifth primary transit after the eclipse observed by Laughlin et al. (2009), comparable to the observed midtransit time of HJD 2454876.344 by Fossey et al. (2009).

4.2. HD 4113b

The planet HD 4113b Tamuz et al. (2008) is a relatively long-period (526.62 days) planet in an eccentric orbit ($e = 0.903$). The periastron argument is $\omega = 317.7^{\circ}$, which results in a secondary eclipse probability of 3.9%. In contrast, the transit probability for this planet is only 0.5%. If this planet were observed to undergo a secondary eclipse, then the subsequent constraints upon the orbital inclination increase the transit probability to an attractive 16.1%.

The long period of this planet's orbit implies an expected transit duration of ~ 19 hr, which produces the observational challenge of attempting to observe either ingress or egress. If a secondary eclipse is observed, then the next predicted transit midpoint will occur only 19.55 days later. Although it is certainly possible to marshal the needed observing resources within that time frame, a missed opportunity will require waiting an entire complete period of 526.62 days before the next chance arrives. Additionally, the similar orbital orientation of HD 4113b to HD 80606b with respect to the observer means that the time between eclipse and periastron is only 1.72 days.

4.3. HD 37605b

The eccentric planet HD 37605b was discovered by Cochran et al. 2004. Since then, the orbital parameters have been revised and published in the catalog by Butler et al. (2006). The orbital

period of 54.23 days, eccentricity of 0.731, and periastron argument of 211.6° yield a secondary eclipse probability of 6.0%. A priori, the transit probability of this planet is 2.6%. The constraints placed upon the inclination if a secondary eclipse is detected raise this probability to an impressive 54.1%.

The relatively short period of this planet make this an attractive target for follow-up campaigns. The time period between periastron passage and the secondary eclipse is 1.09 days. After the secondary eclipse is observed, the possibility of a primary transit will present itself 48.48 days later which should be sufficient time to schedule the necessary follow-up resources.

5. DISCUSSION

There are various factors which we have not included in this analysis that we briefly discuss here. Firstly, the effects of transit timing variations for cases of multiplanet systems has not been considered in the transit/eclipse predictions. This has been discussed in detail by several others, such as Agol et al. (2005) and Holman & Murray (2005). Attempts have been made to detect this effect, such as the monitoring of HD 209458b by the *Microvariability and Oscillations of Stars (MOST)* satellite (Miller-Ricci et al. 2008), but the effect has not been observed at the time of writing. For a given transit, the influence of additional planets on timing variations could be large, depending upon the mass ratio of the planets and the eccentricities of the orbits. In general though, this effect is relatively small (minutes) and is cyclic in nature such that the net effect over many orbits is zero. In addition, many of the more interesting cases discussed in this article are highly eccentric giant planets which tend to be the only known (detectable) planet in those systems.

The second item of note is the issue of how detectable the signature of a secondary eclipse is, both from the ground and from space. The attempt to observe a secondary eclipse is undoubtedly much more difficult than for a primary eclipse due to such factors as the relatively low eclipse depth and the wavelength restriction for optimal detection. Planetary emissions and their associated flux ratios have been discussed in detail by such papers as Charbonneau et al. (2005) and Burrows et al. (2006). In particular, Burrows et al. (2006) have shown that the contrast ratios for hot Jupiters in the mid-IR will be of order $>10^{-3}$. The contrast ratio for longer-period planets will scale with $1/r^2$, in which case r (as defined in eq. [3]) is evaluated at the point of predicted secondary eclipse. The results described in this article assist in evaluating the preferred targets for follow up and whether a difficult observation with high probability (secondary eclipse) may be preferable to a somewhat easier observations with low probability (primary transit), as was the case for HD 80606b.

Finally, we note that the results of this article will be verifiable statistically as more secondary eclipses are detected. This

will be particularly pertinent in upcoming years as the high-precision photometry from such missions as CoRoT and Kepler are released. One such secondary eclipse detection has been observed by CoRoT for the transiting exoplanet CoRoT-2b (Alonso et al. 2009). Though the presence of the eclipse may be expected for such a short-period planet, the sensitivity of Kepler to longer-period planets will result in the detection of secondary eclipses without the necessity of primary transits. The photometric precision of the Kepler photometry is such that, despite the contrast ratios mentioned here, we can expect many such detections from the Kepler mission. The equations described in this article can then be used to assess if and when the primary transit will occur.

6. CONCLUSIONS

Using the known expressions for the a priori probabilities of primary and secondary transits, we have confirmed the literature result that higher eccentricities favor transit and eclipse detections when compared to circular orbits with the same period. Furthermore, we find that higher eccentricities produce a larger range of ω for which both transit and eclipse probabilities are increased with respect to corresponding circular orbits. We show the probabilities of secondary eclipses for the known exoplanets in combination with the range of periastron arguments for which both eclipse and transit probabilities are enhanced. Applying our insight to the planets catalogued by Butler et al. (2006), we find there are several interesting cases that warrant further investigation.

Furthermore, we show that the constraints placed upon the orbital inclination through detection of a secondary eclipse can substantially improve a posteriori estimates of transit probability even with weak constraints upon the impact parameter. For 75% of the planets considered here, the transit probability reaches 100% if a secondary eclipse is observed. We also provide analytical expressions for calculating the time from detected secondary eclipse to the time of predicted primary transit. We present several case studies with relatively high secondary eclipse probabilities with respect to their periods. The planets HD 4113b and HD 37605b present analogous secondary eclipse potential to HD 80606b and we encourage follow up of these targets at predicted secondary eclipse times, provided that the eclipse windows can be sufficiently constrained.

With the picture of planetary atmospheres becoming gradually clearer, the importance of additional eclipsing planets is obvious. For planets with high secondary-eclipse probabilities, the high-risk/high-return strategy of monitoring these planets will reap significant rewards in the growing field of exoplanetary atmospheres.

The authors would like to thank Scott Fleming and Suvrath Mahadevan for several useful suggestions.

REFERENCES

- Agol, E., Steffen, J., Sari, R., & Clarkson, W. 2005, *MNRAS*, 359, 567
- Alonso, R., Guillot, T., Mazeh, T., Aigrain, S., Alapini, A., Barge, P., Hatzes, A., & Pont, F. 2009, *A&A*, 501, L23
- Barbieri, M., et al. 2007, *A&A*, 476, L13
- Barnes, J. W. 2007, *PASP*, 119, 986
- Burke, C. J. 2008, *ApJ*, 679, 1566
- Burrows, A., Hubeny, I., & Sudarsky, D. 2005, *ApJ*, 625, L135
- Burrows, A., Sudarsky, D., & Hubeny, I. 2006, *ApJ*, 650, 1140
- Butler, R. P., et al. 2006, *ApJ*, 646, 505
- Charbonneau, D., et al. 2005, *ApJ*, 626, 523
- Cochran, W., et al. 2004, *ApJ*, 611, L133
- de Mooij, E. J. W., & Snellen, I. A. G. 2009, *A&A*, 493, L35
- Deming, D., Harrington, J., Seager, S., & Richardson, L. J. 2006, *ApJ*, 644, 560
- Deming, D., Richardson, L. J., & Harrington, J. 2007, *MNRAS*, 378, 148
- Deming, D., Harrington, J., Laughlin, G., Seager, S., Navarro, S. B., Bowman, W. C., & Horning, K. 2007, *ApJ*, 667, L199
- Fossey, S. J., Waldman, I. P., & Kipping, D. M. 2009, *MNRAS*, 396, L16
- Garcia-Melendo, E., & McCullough, P. R. 2009, *ApJ*, 698, 558
- Gillon, M., et al. 2009, *A&A*, in press (arXiv:0905.4571)
- Grillmair, C. J., et al. 2008, *Nature*, 456, 767
- Holman, M. J., & Murray, N. W. 2005, *Science*, 307, 1288
- Kane, S. R. 2007, *MNRAS*, 380, 1488
- Kane, S. R., & von Braun, K. 2008, *ApJ*, 689, 492
- Knutson, H. A., et al. 2007, *Nature*, 447, 183
- Laughlin, G., Deming, D., Langton, J., Kasen, D., Vogt, S., Butler, P., Rivera, E., & Meschiari, S. 2009, *Nature*, 457, 562
- Miller-Ricci, E., et al. 2008, *ApJ*, 682, 586
- Moutou, C., et al. 2009, *A&A*, 498, L5
- Naef, D., et al. 2001, *A&A*, 375, L27
- Seager, S., & Mallén-Ornelas, G. 2003, *ApJ*, 585, 1038
- Sing, D. K., & López-Morales, M. 2009, *A&A*, 493, L31
- Tamuz, O., et al. 2008, *A&A*, 480, L33
- Williams, P. K. G., Charbonneau, D., Cooper, C. S., Showman, A. P., & Fortney, J. J. 2006, *ApJ*, 649, 1020
- Winn, J. N., et al. 2009, *ApJ*, 693, 794